

Supporting Information

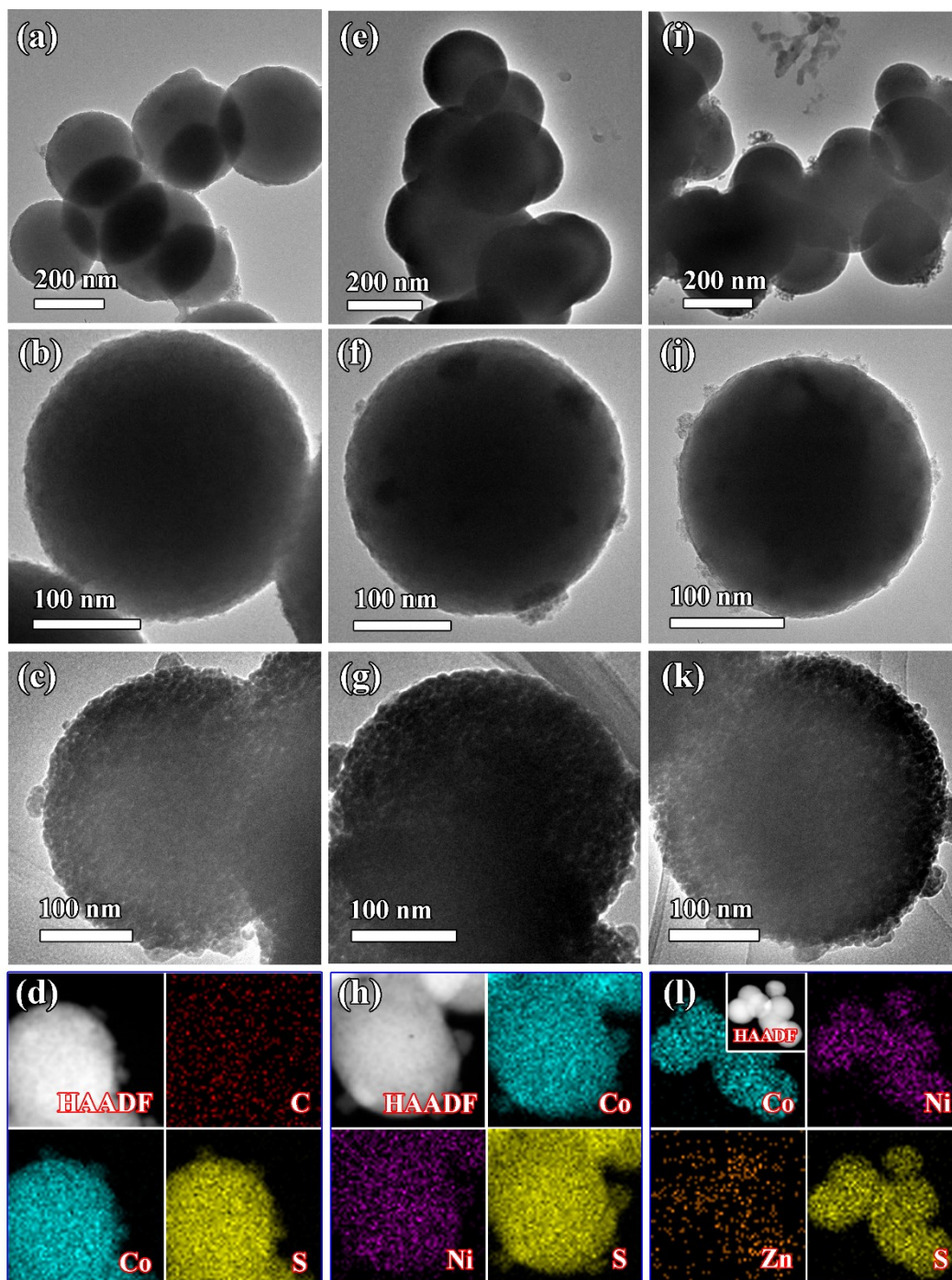


Figure S1 TEM images and corresponding STEM/EDS mapping of (a, b, c, d) CoS₂@C, (e, f, g, h) Ni-CoS₂@C, and (i, j, k) Zn-CoS₂@C spheres. (c, g, k) are TEM images of annealed samples, (l) represent STEM/EDS elemental mapping of Ni/Zn-CoS₂@C spheres confirming low concentration of elemental Zn.

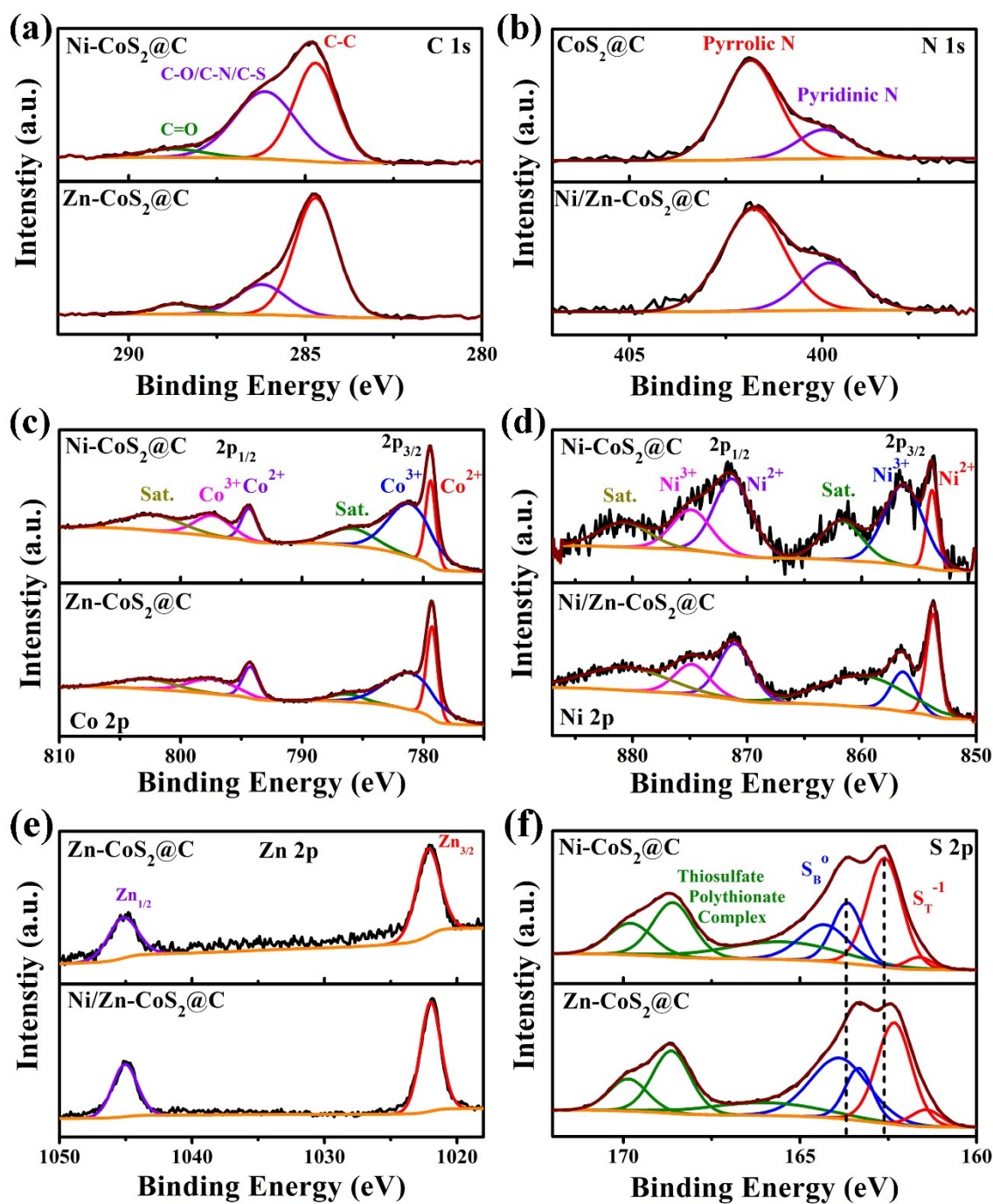


Figure S2 High-resolution XPS spectra of C 1s (a), N 1s (b), Co 2p (c), Ni 2p (d), Zn 2p (e), and S 2p (f) for CoS₂@C, Ni-CoS₂@C, Zn-CoS₂@C, and Ni/Zn-CoS₂@C spheres.

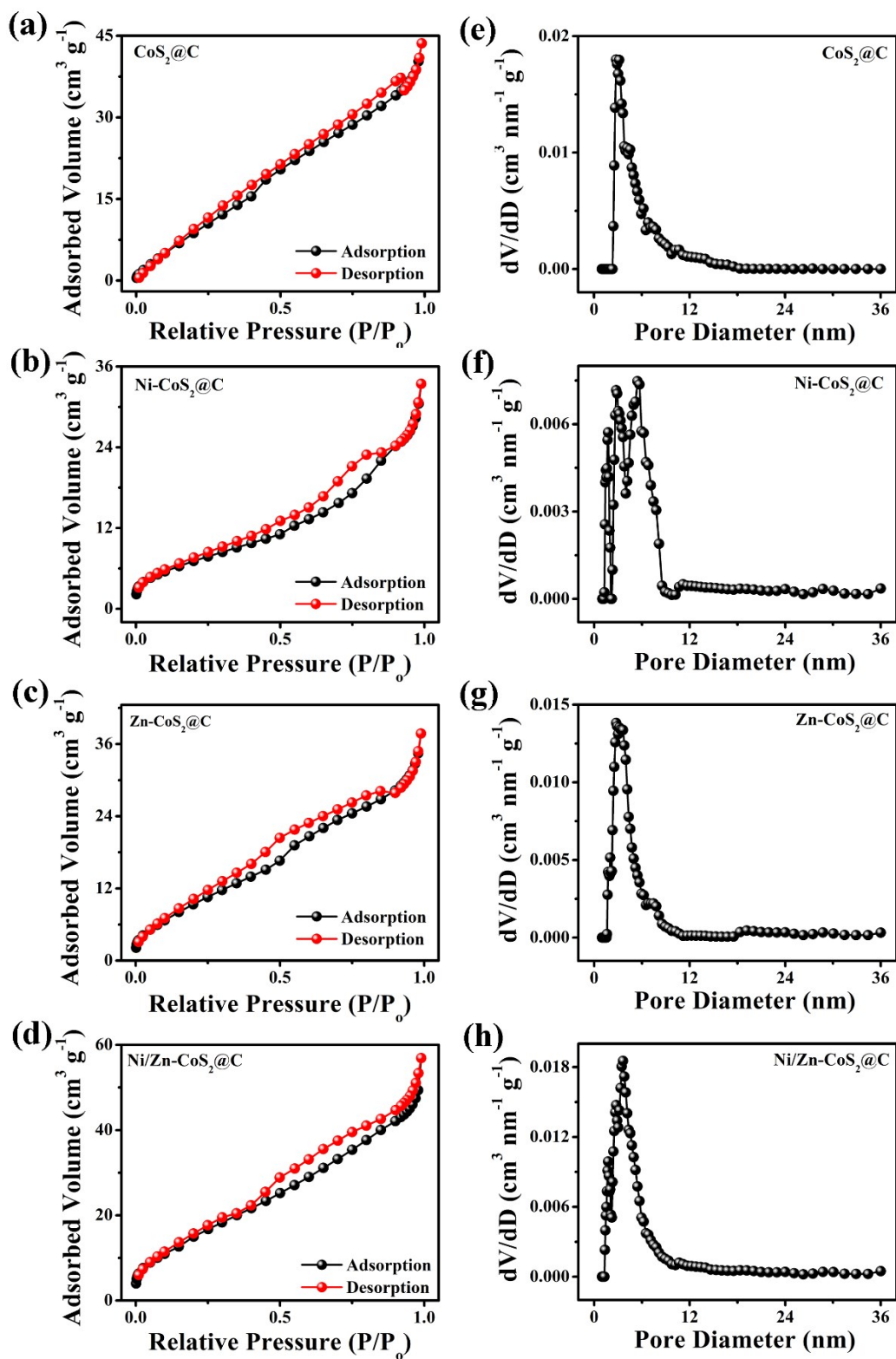


Figure S3 BET nitrogen adsorption-desorption isotherm plots (a, b, c, d) and corresponding pore size distribution (e, f, g, h) of CoS₂@C, Ni-CoS₂@C, Zn-CoS₂@C, and Ni/Zn-CoS₂@C spheres, respectively.

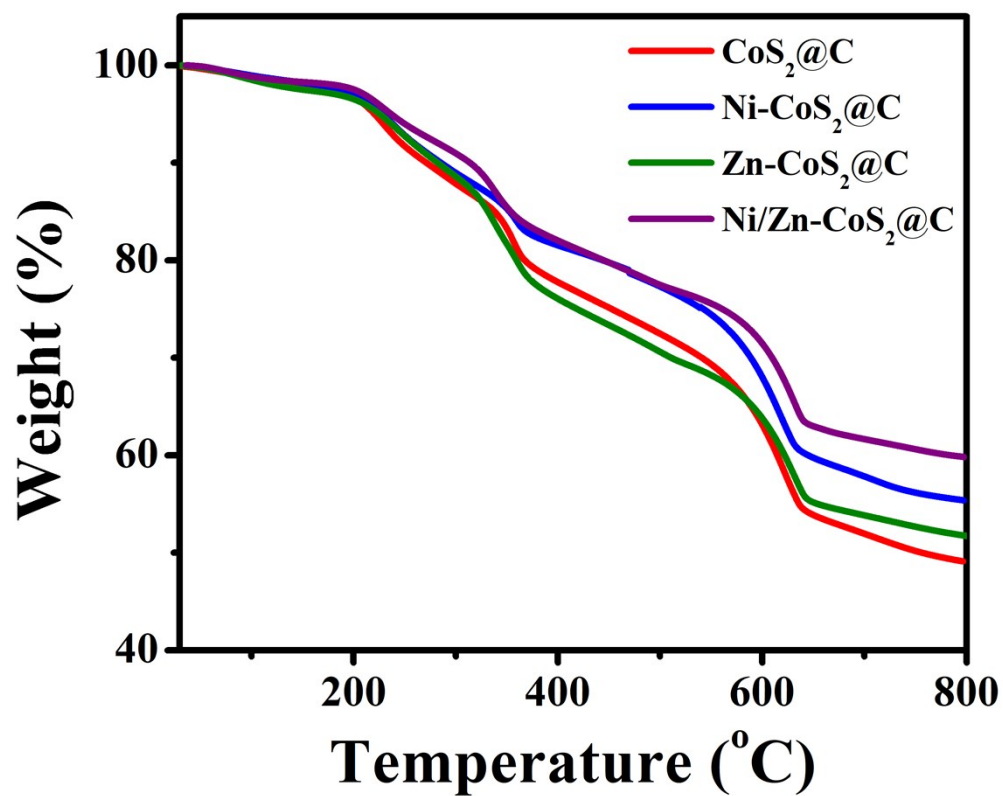
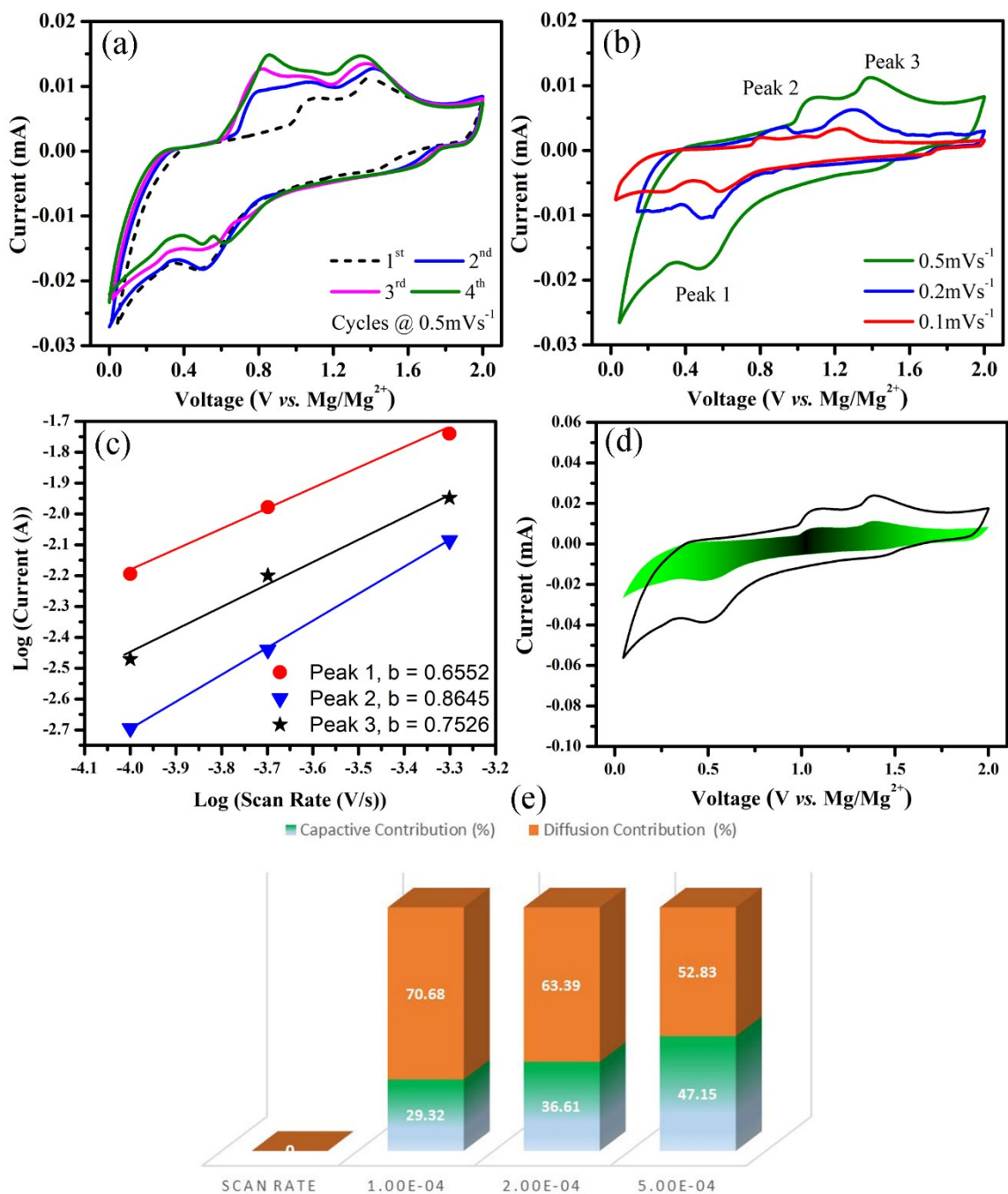


Figure S4 TGA analysis: TGA plot of percentage weight loss with rise in temperature, for CoS₂@C, Ni-CoS₂@C, Zn-CoS₂@C, and Ni/Zn-CoS₂@C spheres.



(d) at 0.5mV.s⁻¹,

Figure S5 Cyclic voltammetry of Zn/Ni-CoS₂@ClAPC //Mg at (a) 0.5 mVs⁻¹, (b) 0.1, 0.2, and 0.5 mVs⁻¹; (c) *b*-value analysis from plot of Log (current) vs. Log (Scan rate); (d) capacitive (shaded area) current contribution to total charge storage at 0.5 mV.s⁻¹, and (e) capacitive and diffusion contribution ratios at different scan rates.

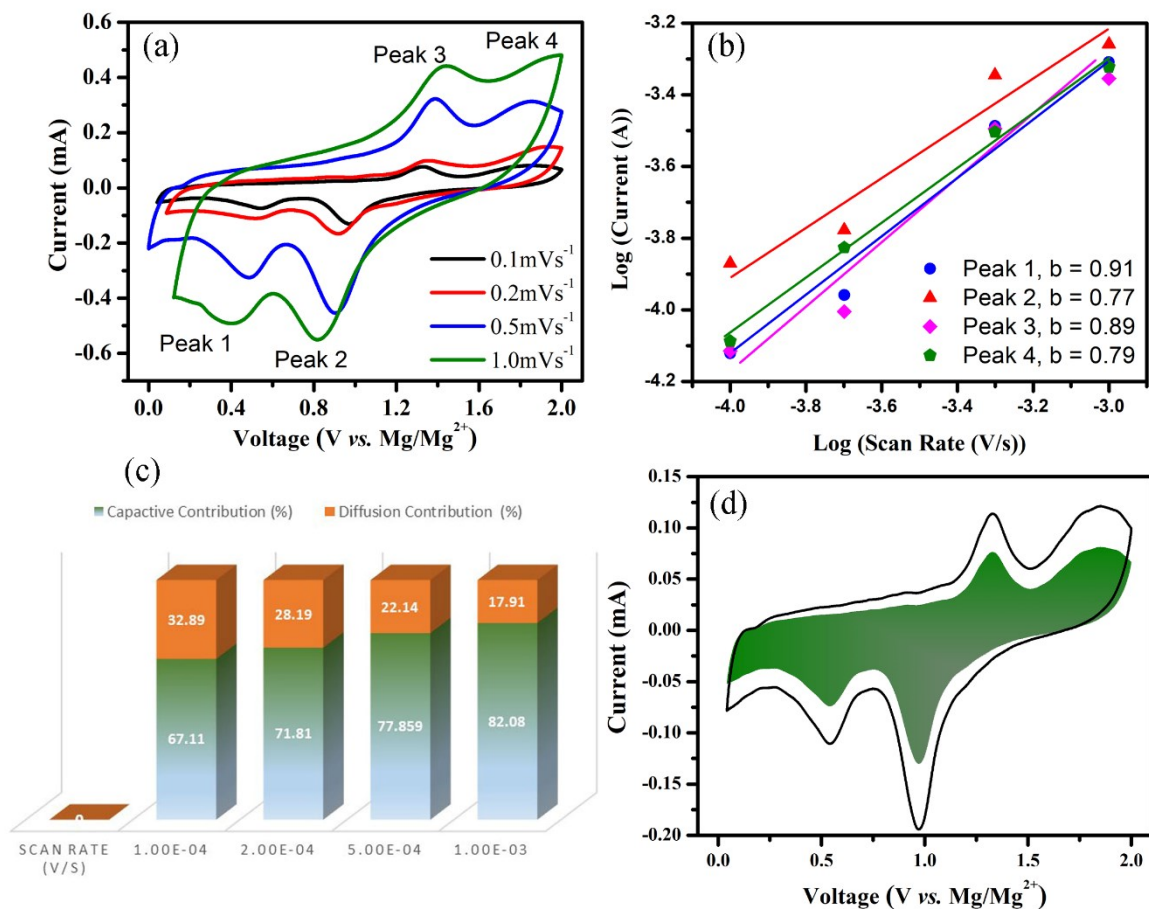


Figure S6 (a) Cyclic voltammetry of Zn/Ni-CoS₂@ClAPC-LiCl|Mg hybrid cell at 0.1, 0.2, 0.5, and 1.0 mV s⁻¹; (b) *b*-value analysis from plot of Log (current) vs. Log (Scan rate); (c) capacitive and diffusion contribution ratios at different scan rates (d) capacitive (shaded area) current contribution to total charge storage at 0.1 mV s⁻¹.

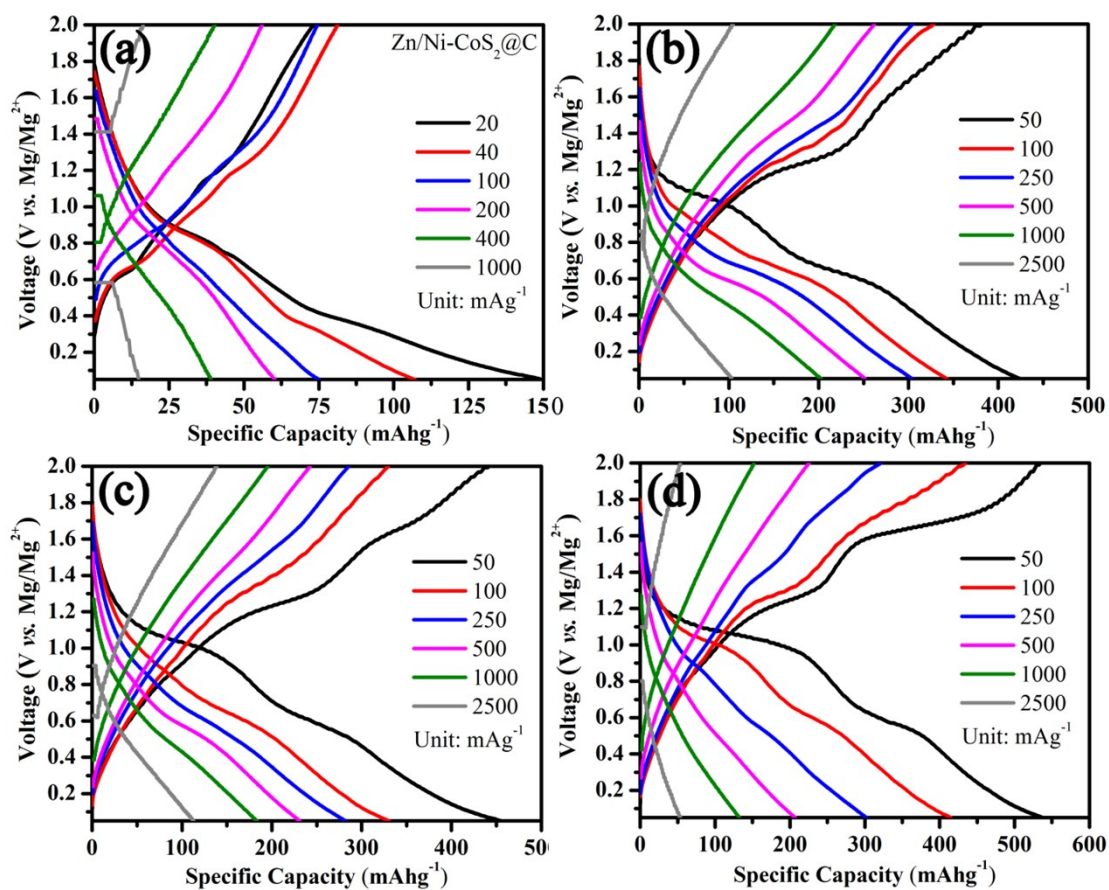


Figure S7 Galvanostatic charging-discharging profiles of (a) Zn/Ni- CoS_2 @C based MIB; (b) CoS_2 @C, (c) Ni- CoS_2 @C, (d) Zn- CoS_2 @C based MLIB at different current densities.

Table S1 Comparison of present work (MLIBs) with conventional LIBs reported in literature.

Cathodes	Maximum Capacity (mA g ⁻¹) [Current Density (mA g ⁻¹)]	Capacity Retention (%) [Number of Cycles]	Reference
CoS ₂ -CNTs	805 [100]	56 [50]	[1]
CoS ₂ -rGO	678 [100]	50 [100]	[1]
CoS ₂ -fCNTs	801 [50]	99 [200]	[2]
CoS ₂	498 [50]	20 [200]	[2]
S/CoS ₂ -NC	950 [100]	75 [250]	[3]
CoS ₂	450 [100]	25 [100]	[4]
CoS ₂ -CNTs	602 [100]	65 [100]	[4]
CoS ₂ -GNs	825 [100]	77 [100]	[4]
CoS ₂ @C	750 [500]	71 [200]	[5]
CoS ₂ -Carbon	815 [100]	63 [120]	[6]
CoS ₂	698 [100]	21 [80]	[7]
Co _{1-x} S@C@rGO	601 [100]	99 [500]	[8]
MnS/Co _{1-x} S@C	700 [100]	99 [500]	[8]
C@Co ₉ S ₈	647 [200]	55 [50]	[9]
CoS ₂ PH	725 [100]	N.A	[10]
CoS PH	590 [100]	N.A	[10]
CoS-rGO	789 [62.5]	72 [100]	[11]
CoS ₂ /CNTs/graphene	604 [100]	67 [100]	[12]
CoS ₂	325 [100]	12 [100]	[12]
CoS ₂ /RGO	788 [100]	87 [50]	[13]
Zn/Ni-CoS₂@C	667 [50]	73 [100]	Present Work

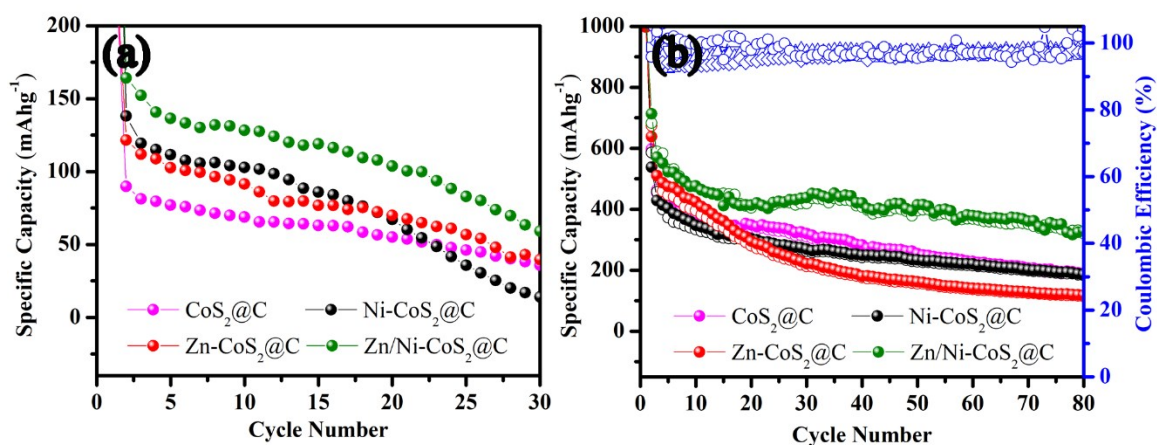


Figure S8 Cycle stabilities of (a) MIBs at 20 mA g⁻¹ and (b) MLIBs at 100 mA g⁻¹.

Table S2 Atomic percentage of different elements in charged (2V), discharged (0.0V), and blank electrodes.

Electrode Status	Elements				
	Co (%)	S (%)	Zn (%)	Ni (%)	Mg (%)
Blank	3.81	10.08	0.84	1.01	0.00
D 0.0V	2.60	2.83	0.65	0.70	5.91
C 2.0V	3.04	4.80	0.53	0.79	1.37

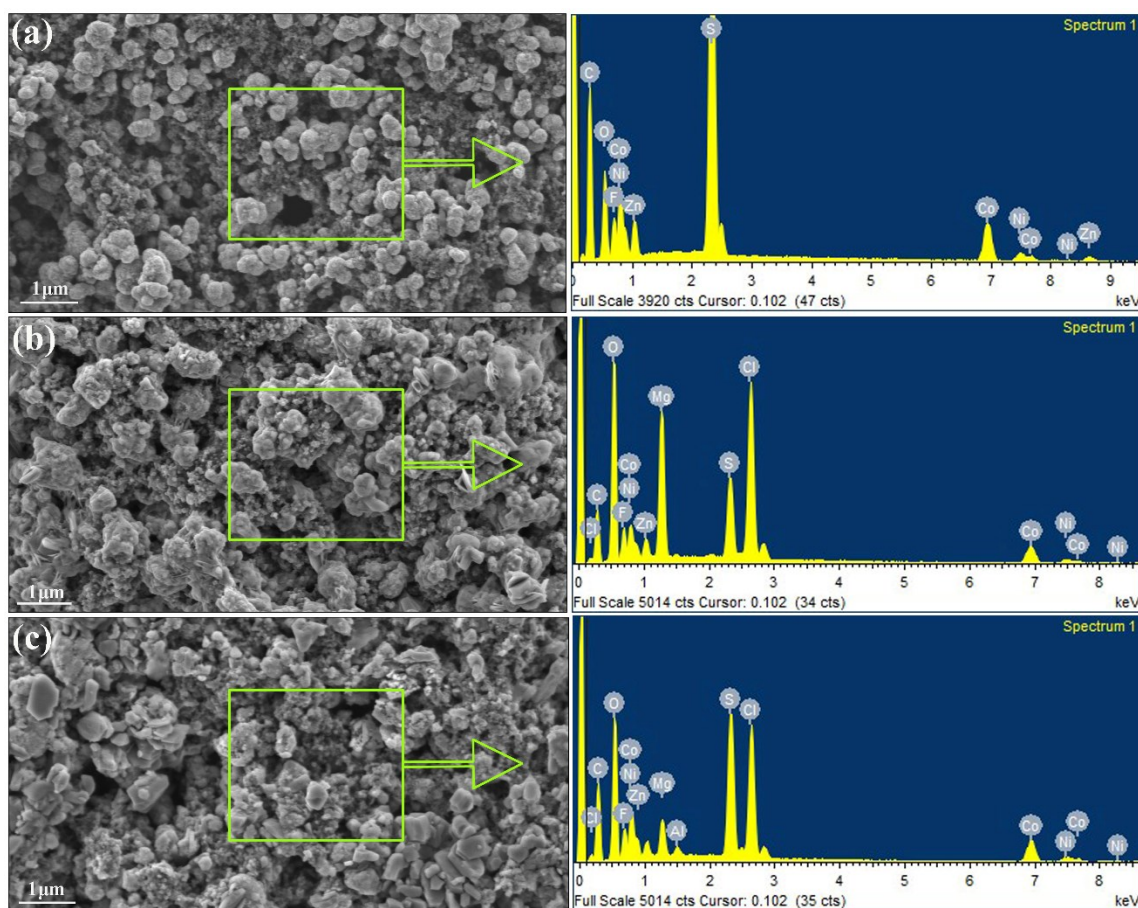


Figure S9 Surface morphology and elemental analysis of Zn/Ni-CoS₂@C cathodes (a) blank, (b) discharged 0.0V, and (c) fully charged 2.0V states.

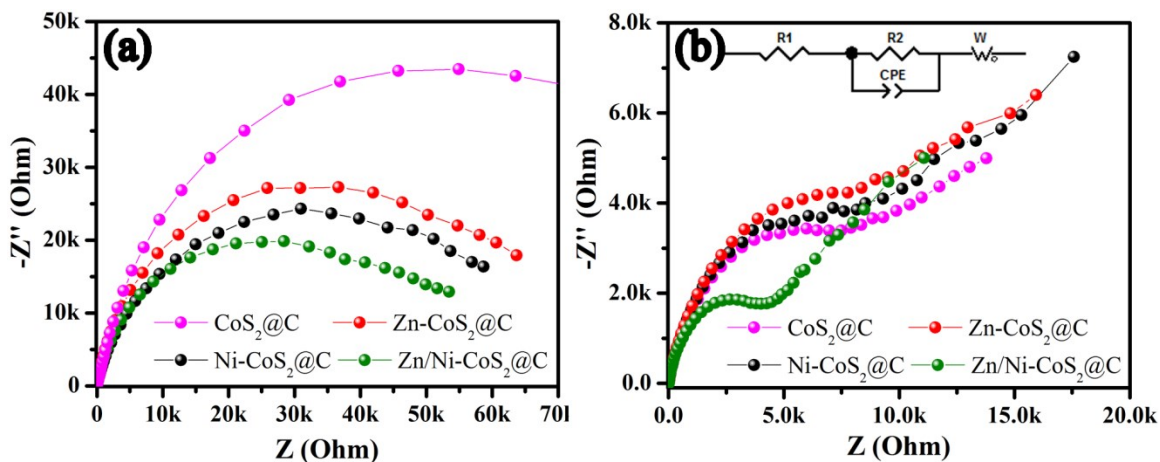


Figure S10 Electrochemical impedance curves of different electrodes at the open circuit potential (a) MIBs; and (b) MLIBs. (Inset in (b) represents the equivalent circuit).

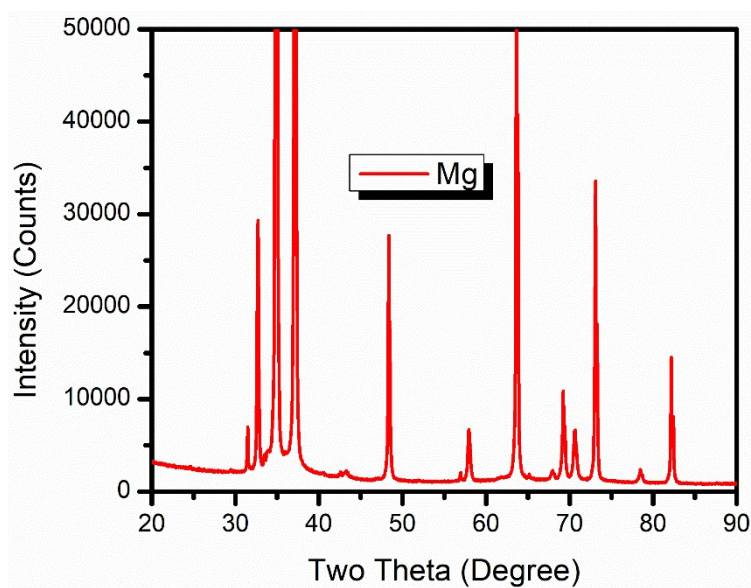


Figure S11 XRD profile of Mg anode after cycling in hybrid electrolytes.

Calculation of Energy and Power Densities:

The power density (***P***) was calculated using Equation 1 given below.

$$P = U * I \quad (1)$$

Where ***U*** is average working voltage of battery and ***I*** is applied current. Whereas, energy density ***E*** was calculated using average working voltage (***U***), specific capacity (***C***) based on the total mass of the active materials (***m***) using Equation 2 given below.

$$E = U * C / m \quad (2)$$

References

- [1] X. Zhu, Z. Meng, H. Ying, X. Xu, F. Xu, W. Han, Chemical Physics Letters 2017, 684, 191.
- [2] Z. X. Huang, Y. Wang, J. I. Wong, W. H. Shi, H. Y. Yang, Electrochimica Acta 2015, 167, 388.
- [3] J. Zhou, N. Lin, W. I. Cai, C. Guo, K. Zhang, J. Zhou, Y. Zhu, Y. Qian, Electrochimica Acta 2016, 218, 243.
- [4] X. Zhang, X. Jie Liu, G. Wang, H. Wang, Journal of Colloid and Interface Science 2017, 505, 23.
- [5] W. Chen, T. Li, Q. Hu, C. Li, H. Guo, Journal of Power Sources 2015, 286, 159.
- [6] Y. Zhang, N. Wang, C. Sun, Z. Lu, P. Xue, B. Tang, Z. Bai, S. Dou, Chemical Engineering Journal 2018, 332, 370.
- [7] J. M. Yan, H. Z. Huang, J. Zhang, Z. J. Liu, Y. Yang, Journal of Power Sources 2005, 146, 264.
- [8] B. Li, R. Wang, Z. Chen, D. Sun, F. Fang, R. Wu, Journal of Materials Chemistry A 2019, 7, 1260.
- [9] W. Shi, J. Zhu, X. Rui, X. Cao, C. Chen, H. Zhang, H. H. Hng, Q. Yan, ACS Applied Materials & Interfaces 2012, 4, 2999.
- [10] Y. Wang, J. Wu, Y. Tang, X. Lü, C. Yang, M. Qin, F. Huang, X. Li, X. Zhang, ACS Applied Materials & Interfaces 2012, 4, 4246.
- [11] Y. Gu, Y. Xu, Y. Wang, ACS Applied Materials & Interfaces 2013, 5, 801.
- [12] C. Xu, Y. Jing, J. He, K. Zhou, Y. Chen, Q. Li, J. Lin, W. Zhang, Journal of Alloys and Compounds 2017, 708, 1178.
- [13] B. Qiu, X. Zhao, D. Xia, Journal of Alloys and Compounds 2013, 579, 372.